Development 134, 4479-4489 (2007) doi:10.1242/dev.008979

Neuronal calcium sensor-1 modulation of optimal calcium level for neurite outgrowth

Kwokyin Hui[1], Guang-He Fei[1], Bechara J. Saab[2,3], Jiang Su[1], John C. Roder[2,3] and Zhong-Ping Feng[1,*]

Neurite extension and branching are affected by activity-dependent modulation of intracellular Ca^{2+}, such that an optimal window of $[Ca^{2+}]_i$ is required for outgrowth. Our understanding of the molecular mechanisms regulating this optimal $[Ca^{2+}]_i$ remains unclear. Taking advantage of the large growth cone size of cultured primary neurons from pond snail *Lymnaea stagnalis* combined with dsRNA knockdown, we show that neuronal calcium sensor-1 (NCS-1) regulates neurite extension and branching, and activity-dependent Ca^{2+} signals in growth cones. An NCS-1 C-terminal peptide enhances only neurite branching and moderately reduces the Ca^{2+} signal in growth cones compared with dsRNA knockdown. Our findings suggest that at least two separate structural domains in NCS-1 independently regulate Ca^{2+} influx and neurite outgrowth, with the C-terminus specifically affecting branching. We describe a model in which NCS-1 regulates cytosolic Ca^{2+} around the optimal window level to differentially control neurite extension and branching.

KEY WORDS: NCS-1, Neurite outgrowth, Activity-dependent calcium signals, fura-2 imaging, *Lymnaea stagnalis*

INTRODUCTION

Neurite extension and branching are affected by activity-dependent modulation of intracellular Ca^{2+} (Komuro and Rakic, 1996; Tang et al., 2003; Zheng, 2000), such that an optimal window of $[Ca^{2+}]_i$ is required (see Gomez and Spitzer, 2000; Henley and Poo, 2004; Kater and Mills, 1991): lower levels stabilize growth cones and higher levels stall them, in both cases preventing extension. Cytosolic Ca^{2+} can come from many sources, including ionotropic receptors, Ca^{2+} channels, Ca^{2+}-release channels and Ca^{2+} pumps (see Berridge et al., 2003). Our understanding of the molecular mechanisms regulating this optimal $[Ca^{2+}]_i$ remains unclear.

Neuronal calcium sensor-1 (NCS-1) is a member of a superfamily of proteins that respond to local Ca^{2+} changes (Ames et al., 1997; Tanaka et al., 1995). It interacts with a variety of proteins that are involved in Ca^{2+} homeostasis (Burgoyne, 2004). In particular, NCS-1 modulation of L- (Rousset et al., 2003), non-L- (Weiss et al., 2000), N- (Rousset et al., 2003; Wang et al., 2001) and P/Q-type Ca^{2+} channels (Rousset et al., 2003; Tsujimoto et al., 2002; Weiss and Burgoyne, 2001) directly changes intracellular Ca^{2+} levels. It also affects intracellular Ca^{2+} concentration directly by modulating Ca^{2+}-permeable transient receptor potential (TRP) channels (Hui et al., 2006) and InsP3 receptor activity (Schlecker et al., 2006), and indirectly by affecting K^+ channel expression and function (Guo et al., 2002; Nakamura et al., 2001). It interacts with signaling-transduction pathways that are known to affect ion channel activity or expression, including dopamine receptors, G-protein dependent receptor kinase 2 (Kabbani et al., 2002) and cyclic nucleotide phosphodiesterase (Schaad et al., 1996), and to regulate exocytosis via phosphatidylinositol-4 kinase β (Kapp-Barnea et al., 2003; Taverna et al., 2002; Zhao et al., 2001). Thus, NCS-1 is a likely candidate for dynamically regulating cytosolic Ca^{2+} levels.

[1]Department of Physiology, and [2]Molecular and Medical Genetics, Faculty of Medicine, University of Toronto, Toronto, M5S 1A8, Canada. [3]Mount Sinai Hospital, Toronto, Canada.

*Author for correspondence (e-mail: zp.feng@utoronto.ca)

Accepted 13 September 2007

There is compelling evidence that NCS-1 is involved in neurite development in a few systems. For instance, NCS-1 expression increases in grey matter and decreases in white matter during embryogenesis and early postnatal stages (Kawasaki et al., 2003). Overexpression of NCS-1 in NG108-15/rat myotube co-cultures (Chen et al., 2001), and of the *Drosophila* homologue Frequenin (Frq) in motor nerve terminals (Angaut-Petit et al., 1998), reduces the number of neurites. More recently, NCS-1 was shown to impede neurite extension without altering branching in NGF-treated PC12 cells by potentiating TRPC5-evoked Ca^{2+} currents (Hui et al., 2006). However, there has been no study to examine if and how NCS-1 is involved in regulation of the window level of Ca^{2+} permissive to neurite outgrowth.

In this study, we examined the affects of NCS-1 on intracellular Ca^{2+} and neurite outgrowth in cultured *L. stagnalis* snail PeA neurons. Using RNA interference, we found that *NCS-1* knockdown enhanced neurite extension and branching, and reduced activity-dependent Ca^{2+} influx in growth cones. Using a C-terminal peptide of NCS-1, we show that the C-terminus modulates growth cone whole-cell voltage-dependent Ca^{2+} currents and enhances neurite branching. Our findings indicate that NCS-1 modulates neurite branching and extension by regulating Ca^{2+} influx through at least two mechanisms: one that specifically affects branching, and another that specifically affects extension.

MATERIALS AND METHODS

Animal and primary cell culture

Freshwater pond snails, *L. stagnalis*, were obtained from an inbred stock maintained at the Free University in Amsterdam, and were raised and maintained at the University of Toronto under a 12 hour light/dark cycle in aquaria containing 20°C water. All animals used in these studies were fed green leaf lettuce twice a week. Serotonergic Pedal A (PeA) neurons, which are involved in locomotion and are found in each pedal ganglion in clusters of approximately 30 cells (Spencer et al., 1995), were isolated as previously described (Feng et al., 1997; Syed et al., 1990). Briefly, 2-month-old snails having shell lengths of 15 to 20 mm were anesthetized for 10 minutes with 10% (v/v) Listerine. The central ring and the buccal ganglia were dissected from the snail in sterile snail saline, containing 51.3 mM NaCl, 1.7 mM KCl, 4.1 mM $CaCl_2$, 1.5 mM $MgCl_2$, adjusted to pH 7.9 using 1 M HEPES/NaOH (pH 8.05), and then incubated with 3 mg/ml trypsin (Type

III, Sigma, ON, Canada) for 22 minutes. PeA neurons were isolated individually with gentle suction using a fire-polished Sigmacoted (Sigma, Ontario, Canada) pipette (2 mm, WPI, 1B200F), and subsequently transferred to a poly-L-lysine coated culture dish, where they were maintained in conditioned medium (CM) at room temperature for 24-36 hours. CM was prepared by incubating *L. stagnalis* brains in defined medium (DM) as previously described (Feng et al., 1997; Syed et al., 1990). The DM contained serum-free 50% (v/v) Liebowitz L-15 medium (GIBCO, Grand Island, NY), supplemented with 51.3 mM NaCl, 1.7 mM KCl, 4.1 mM $CaCl_2$, 1.5 mM $MgCl_2$, 10 mM glucose, 1.0 mM L-glutamine and 20 mg/ml gentamycin. The pH of this medium was adjusted to 7.9 with 1 M HEPES/NaOH (pH 8.05).

Cloning

mRNA was extracted from three snail central ring ganglia using the Qiagen RNeasy Mini Kit (Qiagen, Ontario, Canada). We first cloned a partial fragment of *L. stagnalis NCS-1* using first-strand cDNA using Transcriptor reverse transcriptase (Roche Applied Sciences, Quebec, Canada) primed with random 9-mers at 40°C for 25 minutes, then incubated at 70°C for 2 hours. PCR reactions (25 μl) contained cDNA, forward (5′-TACAARC-AGTTCTTCCCATTTGGAGACCC-3′) and reverse (5′-CCATCGTT-ATCCAGATCATACAGAYKRAANGCCCA-3′) degenerate primers, to generate an amplicon of ~300 bp. The PCR cycle consisted of a 10-minute enzyme-activation step at 94°C, followed by 45 cycles of 30 seconds at 94°C, 30 seconds at 60°C, and 2 minutes at 70°C, with a final extension step at 70°C for 3 minutes. Utilizing the forward primer, DNA sequencing confirmed the identity of the PCR product. Cloning of the full-length *NCS-1* gene was by 3′ and 5′ rapid amplification of cDNA ends (RACE) following the SuperSMART PCR cDNA Synthesis Kit (Clontech, Mountain View, CA) in a two-step PCR protocol with some changes. First-strand cDNA was synthesized as described in the kit using the included SMART CDS primer, followed by amplification with the included primer 2A. In the first PCR step, a gene-specific primer (Table 1) was designed based on the partial clone and run with primer-1 (5′-CGACGTGGACTATCCATG-AACGCAAAGCAGTGGTATCAACGCAGAGT-3′), which overlaps with the 5′ end of primer 2A. In the second PCR step, a nested gene-specific primer (Table 1) was designed based on the partial clone and run with primer-2 (5′-TCGAGCGGCCGCCCGGGCAGGTCGACGTGGACTA-TCCATGAACGCA-3′), which overlaps with the 5′ end of primer-1. The 5′ end was cloned in a similar manner, except that a modified random 15-mer (5′-AAGCAGTGGTATCAACGCAGAGTACNNNNNNNNNNNNNNN-3′) was used to prime first-strand synthesis in a reverse transcription at 25°C for 10 minutes prior to a 42°C incubation for 90 minutes. The PCR cycle used in RACE consisted of a 5 minute enzyme-activation step at 94°C, followed by 30 cycles of 30 seconds at 94°C, 30 seconds at 55°C, and 3 minutes at 72°C, with a final extension step at 72°C for 5 minutes. RACE products were confirmed by sequencing. Table 1 lists the gene-specific primers used in RACE. A full-length clone of 704 bp was cloned, coding for a 191 amino acid protein (GenBank DQ099793).

Synthesis of dominant-negative NCS-1 peptide

Peptides were synthesized at the Advanced Protein Technology Centre in Toronto, Canada. The C-terminal NCS-1 peptide (CTN) construct, which consisted of an N-terminal tyrosine ligated to the HIV TAT (YGRKKRRQRRR) protein transduction domain joined by a tetra-glycine spacer [$(Gly)_4$] at its C-terminus to the 34 amino acid sequence found at the C-terminus of NCS-1 (DKNADGKLTLQEFQEGSKADPSIVQAL-SLYDGLV), was cleaved from the preparatory column and acetylated. CTN does not contain a complete EF-hand Ca^{2+}-binding motif (Tsujimoto et al., 2002), and does not bind Ca^{2+} (data not shown). To add a fluorescent tag to CTN, BODIPY 499/508 (Molecular Probes, Ontario, Canada) was attached to a Cys residue that had been added to the N-terminus of CTN. The scrambled control peptide (srCTN) was constructed similarly to CTN except that the NCS-1 control peptide previously described (DIDGDGQVNYEEFVQDTLASLSKLAKGLKALPQS) was substituted for the C-terminal NCS-1 region (Tsujimoto et al., 2002). These membrane-permeant CTN constructs allowed us to perform non-invasive studies on the effects of the NCS-1 C-terminus on neurite outgrowth. The N-terminal HIV-1 TAT protein transduction domain (PTD) conferred membrane permeability to the CTN (Vives et al., 1997). CD spectroscopy in the presence of trifluoroethanol indicated the presence of stable α-helices in the CTN at room temperature, similar to those seen in the NCS-1 C-terminus (not shown), indicating that the TAT PTD domain did not alter the conformation of the rest of the peptide.

dsRNA construct

Based on the *L. stagnalis* NCS-1 sequence we cloned, we designed a 27-mer *NCS-1*-specific dsRNA using SciTools RNAi Design software (IDT DNA); we purchased this dsRNA from IDT DNA (Kim et al., 2005). TriFECTa control dsRNA was used as a control in our experiments (IDT DNA). The sequences for each dsRNA are as follows: LNCS dsRNA 5′GUCCUUAUUCUCGUCGAAGACGUUGAA/5P-CAACGUCUUCG-ACGAGAAUAAGGd AdC, TriFECTa control 5′UCACAAGG-GAGAGAAAGAGAGGAAGGA/5P-CUUCCUCUCUUUCUCUCCCU-UGUdGdA, where 5P represents a 5′ phosphate, and dN represents a deoxynucleotide; the other bases in these 27-mers were ribonucleotides. For whole animal knockdown experiments, snails were pinned onto a dissection board, and injected in the head, above the central ganglia, with 2 μl of 20 μM *NCS-1* dsRNA, control dsRNA or 2 μl water. Two days after the injections, animals were sacrificed and separated for western blot analyses into four groups of two for each treatment.

Western blot analysis

Protein extracts were prepared from snail ganglia and from rat brain (Sprague-Dawley, Charles River Lab, Wilmington, MA). Western blots were performed using NuPAGE Novex Bis-Tris Gel (Invitrogen, Ontario, Canada) following the manufacturer's instructions. Specifically, extract samples containing 20 μg protein were separated by electrophoresis on a NuPAGE Novex Bis-Tris Gel in MES running buffer, and were then electrophoretically transferred from the gel to a 0.2 μm PVDF membrane (Invitrogen). Membranes were incubated with 5% blocking solution overnight at 4°C, followed by incubation with rabbit polyclonal anti-rat NCS-1 antibody (diluted 1:500; Biomol, Plymouth Meeting, PA) in 3% blocking solution for 2 hours at room temperature. After washing, membranes were incubated with horseradish peroxidase-conjugated rabbit secondary antibody (diluted 1:5000; Chemicon, Temecula, CA) in 3% blocking solution for 2 hours at room temperature. Antibody-labelled protein bands were visualized using an enhanced chemiluminescent reagent (Amersham Biosciences, Ontario, Canada), and analyzed by scanning densitometry with Kodak 1D image analysis software (Eastman Kodak, USA). Mouse anti-actin antibody (1:500; Chemicon, CA) was used as a control.

Immunocytochemistry and confocal imaging

Cultured PeA cells were fixed with 1% paraformaldehyde in snail saline solution lacking NaCl overnight at 4°C. Cells were then washed three times with snail saline, and incubated with rabbit polyclonal anti-rat NCS-1 antibody (diluted 1:300) in snail saline solution containing 0.3% Trition X-100 and 0.5% BSA overnight at 4°C. Following three washes with snail saline, cells were incubated with FITC-conjugated anti-rabbit secondary antibody (diluted 1:600; Chemicon) for 2 hours at 20°C. After three washes with snail saline, and one wash with distilled water, the preparation was

Table 1. Primers used to clone the full-length gene for *L. stagnalis NCS-1*

RACE	Gene-specific primer	Nested gene-specific primer
5′	CGTCACGGACAAGGCTTG	CCTTTGTGCCATTGTTTGATCTC
3′	GATGCTATTTATAGAATGGTGGGAG	GAATGGTGGGAGAATCAGTAACATTAC

Sequences are listed 5′ to 3′.

mounted with permafluor (Fisher Scientific, Canada). Confocal images of NCS-1 reactivity were acquired using a TCS SL laser confocal microscope (Leica Confocal Software, version 2.5, build 1347, Leica Microsystems, Germany). *z*-series scan images of labelled cells were viewed under a 40× oil immersion lens using a He-Ne laser. The FITC-conjugated fluorophore was excited at 483 nm, and peak intensity emissions were determined at 543 nm. *z*-series scans of the cells were performed at a zoom level that afforded the largest possible view of cells and their neurites. Each plane was averaged three times using a step size between each plane of approximately 0.5 μm. Background fluorescence was determined using three regions not encompassing cells throughout the entire *z*-stack. Confocal data were analysed using LCS Lite Leica Confocal Software. In the double-labelled experiments, in addition to the rat-NCS-1 antibody, mouse β-actin antibody (diluted 1:500; Chemicon) was also incubated with the cells followed by Alexa-568-conjugated goat anti-mouse antibody (diluted 1:800; Molecular Probes) in the same manner as the rat NCS-1 antibody.

Neurite growth

PeA cells were cultured in CM at 20°C for 24-36 hours. Cells were then treated without or with 5 nM *NCS-1* dsRNA, 5 nM control dsRNA, 50 μM CTN or 50 μM scrambled CTN. Neurite growth pattern images were collected at the time of treatment, and at several later timepoints, through 22 hours, using an Olympus inverted microscope (CK X41) with an Olympus C5050 digital camera. Images were analysed using ImageTool 3.1 software. We considered branches to be outgrowths when segments were longer than 10 μm. Using the 40× objective, neurite lengths were measured from the edge of the somata to the visible tip of the growth cone. Neurite extension rates were defined as the difference between the current and previous lengths divided by the time elapsed between the two measurements.

Intracellular recording and ratiometric fura-2 Ca^{2+} imaging

Intracellular Ca^{2+} ($[Ca]_i$) was measured as described previously using a fura-2 ratiometric Ca^{2+} imaging system (Feng et al., 2002). Cells were incubated for 30 minutes with 4 μM Fura-2 AM (Molecular Probes), and then washed with snail saline three times before imaging. The experiments were carried out in the dark to prevent photobleaching of the dye. Fura-2 was alternately excited at 340 and 380 nm by illumination generated by a 100 W Hg/Xe-arc lamp that had passed through 340 and 380 nm excitation filters; this process was controlled by Image Pro 5 software (PTI). The fluorescence signal was reflected via a 430 nm dichroic mirror, passed through a 510 nm emission filter and detected and digitized by an intensified charged-coupled device (ICCD) camera (Roper Scientific) in Image Pro 5 at 1-10 Hz. The fluorescence intensity (Poenie-Tsien) ratios of images acquired at 340 and 380 nm were calculated using Image Pro 5. Cells were stimulated by action potentials generated by 1 second depolarizing current pulses (Axopatch 700B controlled by Clampex, Axon Instruments) from a sharp electrode containing a saturated solution of KCl or K_2SO_4. The number of action potentials used was controlled by changing the amplitude of the current pulses. The fluorescent signal evoked by the action potentials was recorded with a time-lapse protocol. The peak fluorescent signal was measured and compared under various conditions. The bath solution was composed of snail saline. The fluorescence ratio intensity (340:380) was estimated as described by Grynkiewicz et al. (Grynkiewicz et al., 1985), assuming a K_d of 224 nM.

Voltage-clamp recording

Whole-cell (ruptured) patch-clamp recordings were performed on growth cone regions using an Axopatch 700A amplifier connected to an analogue-to-digital interface Digidata 1322 that was linked to a personal computer running pClamp9 (Axon Instruments, Foster City, CA). Patch pipettes (Sutter borosilicate glass, BF 150-86-15; Novato, CA) were pulled using a Sutter P-87 microelectrode puller, and subsequently fire polished using a Narashige microforge (Narishige), as described previously (Hui et al., 2005). Pipettes (4-10 MΩ) were filled with solution, containing 29 mM CsCl, 2.3 mM $CaCl_2$, 2 mM MgATP, 0.1 mM GTP-Tris, 11 mM EGTA and 10 mM HEPES, adjusted to pH 7.4 with CsOH. Currents were recorded during perfusion with a Ca^{2+} solution containing 10 mM $CaCl_2$, 45.7 mM TEA-Cl, 1 mM $MgCl_2$, 10 mM HEPES and 2 mM 4-AP, adjusted to pH 7.9 with TEA-OH. Currents were elicited by stepping from a holding potential of –100 mV to the test potential using Clampex (Axon Instruments).

Growth cones were transected with a glass pipette and included adjacent neurite. srCTN, or CTN, was added to the cell-culture dish, and sometimes the recording pipette solution. Data were filtered at 1 kHz (–3 dB) using a 4-pole Bessel filter, and digitized at a sampling frequency of 2 kHz. Data were analysed using Clampfit (Axon Instruments). All curve fittings were carried out using Origin 7 (Microcal Origin, MA). Current-voltage relations were fit to the modified Boltzmann equation: $\{1/[1+\exp(-(V-V_h)/S)]\}*(V-V_{rev})*G$, where V is the applied voltage, V_h is the half-activation voltage, S is the slope factor, V_{rev} is the reversal potential and G is the slope conductance. All experiments were performed at room temperature (20-25°C).

Data analysis and statistics

Unless otherwise stated, data are presented as the mean±s.e.m. Statistical analyses were carried out using SigmaStat 3.0 (Jandel Scientific, Chicago, IL). Differences between mean values from each experimental group were tested using a Student's *t*-test for two groups or one-way analysis of variance (ANOVA, Holm-sidak or Tukey method) for multiple comparisons. Differences were considered significant if $P<0.05$.

RESULTS

Expression of NCS-1 protein in *L. stagnalis* neurons

NCS-1 is believed to be highly conserved across species (Burgoyne, 2007). Using degenerate primers corresponding to sequences in a conserved region between the second and third EF-hands of NCS-1 (see Materials and methods), we amplified a ~300 bp DNA segment from *L. stagnalis* brain. This was followed by 5′ and 3′ RACE to yield a gene encoding for a 191 amino acid protein (GenBank Accession no. DQ099793). The sequence of this *L. stagnalis* protein is most similar to that of the *Aplysia californica* aplycalcin protein (Dyer et al., 1996) (95% identity) and very similar to the sequences of other known NCS-1 orthologues (Fig. 1A). To further confirm that the *L. stagnalis* NCS-1 protein is structurally conserved with those of its mammalian counterpart (also known as Freq), we used a rabbit polyclonal anti-rat NCS-1 antibody in western blots of snail brain protein preparations and in immunocytostaining of isolated cells (see below). In the western blots, a strong single band was detected migrating at a rate similar to that of rat NCS-1 (17-28 kDa, Fig. 1B). These results confirm that NCS-1 is highly conserved between species.

If NCS-1 is involved in neurite outgrowth, it should be expressed in growth cones. We examined the expression pattern of NCS-1 in *L. stagnalis* pedal A (PeA) neurons by immunocytochemistry and confocal fluorescence imaging. PeA neurons cultured for 3 days in CM showed NCS-1 immunoreactivity in neurites and soma (Fig. 1C). In contrast to previous studies (Bourne et al., 2001; O'Callaghan et al., 2002), immunoreactivity was diffusely distributed throughout the cytosol rather than being most intense in the membranes. This pattern is similar to that seen in *Aplysia* (Dyer et al., 1996) and may indicate that the N-terminal myristoylation domain, which mediates membrane localization for other NCS proteins (Ames et al., 1995), is concealed at resting levels of Ca^{2+}. Relative to primary neurites (Fig. 1D, $n=5$), NCS-1 expression levels were significantly higher in somata (2.95±0.39, $P<0.05$), growth cones (1.89±0.1, $P<0.05$) and branch points (1.91±0.3, $P<0.05$). Secondary neurites showed slightly higher levels (1.27±0.3) but not significantly different from those observed in primary neurites. The higher levels of NCS-1 observed in growth cones and branching points reaffirm the notion that the protein is involved in neurite outgrowth.

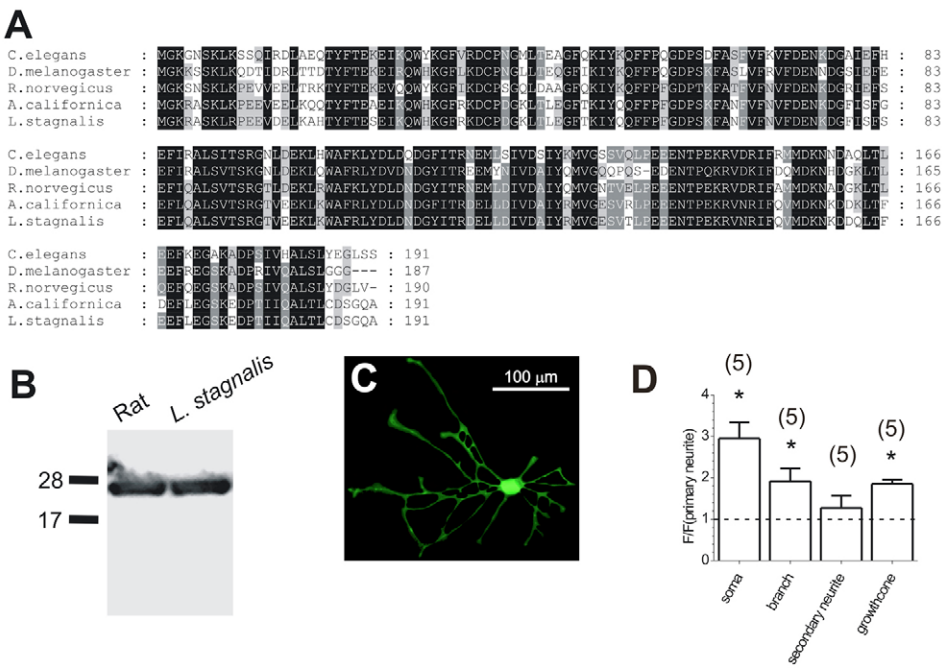

Fig. 1. An NCS-1-related protein is expressed in *L. stagnalis* neurons. (**A**) Protein sequence alignment of the full NCS-1 clone from *L. stagnalis* (DQ099793) and the homologous proteins from *A. californica* (Q16981), *Rattus norvegicus* (P62168), *Drosophila melanogaster* (NP_996502) and *Caenorhabditis elegans* (P36608). Alignment was performed in ClustalW and the plot made in GeneDoc. (**B**) Western blot analysis of whole *L. stagnalis* and rat brains. Polyclonal anti-rat NCS-1 antibody identified a single band migrating at ~23 kDa in both rat and *L. stagnalis* ganglia preparations. (**C**,**D**) Confocal imaging of anti-NCS-1 reactivity in a *L. stagnalis* PeA neuron cultured for 3 days in CM. Epifluorescent image of PeA cell stained with the anti-rat NCS-1 antibody show immunoreactivity throughout the neuron (C). Analysis of cellular distribution of NCS-1 reactivity in the different regions of the cell (D, n=5 cells). The data are presented as mean±s.e.m. Asterisk indicates a significant difference (P<0.05) compared with that in the primary neurites. Relativity intensities compared to primary neurites are 2.95±0.39 for soma, 1.91±0.31 for branch points, 1.27±0.29 for secondary neurites and 1.85±0.10 for growth cones.

NCS-1 knockdown affects both neurite elongation and branching

We next examined how NCS-1 affects neurite outgrowth by using a 27-mer *NCS-1*-specific dsRNA molecule to knockdown the gene. Although the 27-mer design has been well established in mammalian systems (Kim et al., 2005), its usefulness in invertebrates is unclear. We evaluated the effectiveness of this dsRNA in gene silencing by injecting 2 μl of either the *NCS-1* dsRNA (20 μM), or a control dsRNA (20 μM), into the snail central ganglia and examined the protein level from brain protein extracts 2 days later. The *NCS-1* dsRNA treatment, but not control dsRNA treatment, significantly reduced the expression of NCS-1 protein by 35.7±5.1% of the mock group (P<0.05, n=4) without affecting that of β-actin (Fig. 2A,B). No significant difference was found in NCS-1 expression between the control and mock groups.

We studied the effects of the *NCS-1* dsRNA on individually isolated *L. stagnalis* PeA neurons by adding it to the culture medium, thereby avoiding potential cytotoxic or secondary effects of more invasive methods. The expression level of NCS-1 was determined to ensure that the strategy was effective. In cells treated with 5 nM dsRNA for 24 hours, the level of NCS-1 was substantially reduced in all regions relative to β-actin (Fig. 2C,D). As with the in vivo ganglial knockdown results, the relative expression level of NCS-1 to β-actin in the different regions was significantly decreased by ~30% after the *NCS-1* dsRNA treatment (soma 0.84±0.06, n=15; neurite 0.94±0.13, n=6; branching point 0.97±0.08, n=8; and growth cone 1.10±0.16, n=5; P<0.05) compared with the control dsRNA (soma 1.48±0.08, n=10; neurite 1.51±0.12, n=6; branching point 1.44±0.05, n=4; and growth cone 1.60±0.12, n=6). Because the knockdown was only partial, we anticipate that any functional differences we saw in dsRNA and control treatments reflect only a ~30% reduction in NCS-1.

Having established the effectiveness of the dsRNA treatment, we examined the effects of *NCS-1* knockdown on neurite outgrowth. The neurons were grown for 24 hours after isolation in order to allow for recovery and some neurite growth to which we could compare. The cells were subsequently treated with 5 nM dsRNA (*NCS-1*, control or mock) or water (mock) and allowed to grow for another 24 hours. The relatively short treatment period was appropriate in order to minimize variations arising from changing conditioned media, which was necessary due to evaporation. Even with only 24 hour treatment with the *NCS-1* dsRNA, there was significant reduction in NCS-1 expression (Fig. 2) and change in the neuron morphology (Fig. 3A).

NCS-1 knockdown altered both neurite branching and extension in the cultured neurons. Many cells did not sprout neurites during the first 24 hours before dsRNA-treatment, and were not examined further. Of the remaining cells, the number of newly formed neurite branches after *NCS-1* dsRNA treatment (3.9±0.6, n=57 cells) was significantly larger than the control dsRNA (1.0±0.3, n=43 cells) and the mock control (1.5±0.4, n=24 cells) treatments (Fig. 3B). We measured the length of the neurites before and after the treatments, and found that 75 to 80% of the neurites advanced and the remaining neurites either retracted or remained unchanged during the period of treatment (24 hours). The fraction of neurites which advanced was not affected by the treatments. As the *NCS-1* dsRNA treatment altered the degree of branch of the neurons and extension

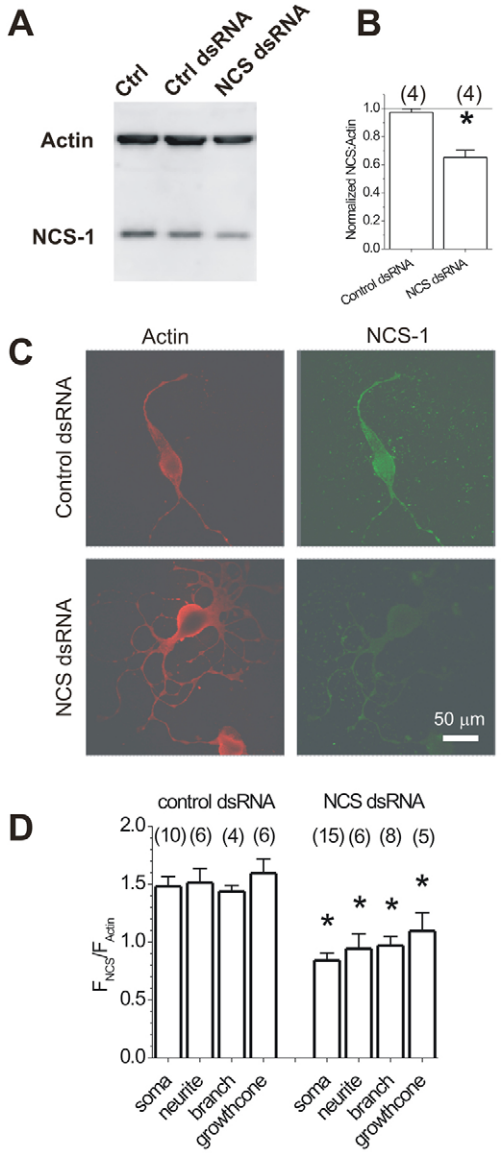

Fig. 2. 27-mer dsRNA knockdown of NCS-1 in *L. stagnalis*. (**A**,**B**) Western blot analysis of ganglia protein extracts isolated 2 days after the snails were injected with either *NCS-1* dsRNA (*NCS* dsRNA), control dsRNA (Ctrl dsRNA) or water (Ctrl), showing that *NCS-1* dsRNA reduced the protein level of NCS-1. (A) Representative semiquantitative immunoblots of NCS-1 and β-actin expression in the central ganglia with indicated pretreatments. (B) A summary of normalized intensity of NCS-1 to β-actin ratio from dsRNA-treated groups compared with that from the control group. The solid line indicates the NCS-1 to β-actin ratio of the control group. *NCS-1* dsRNA treatment (2 μl of 20 μM) resulted in an average 35.7±5.1% (*n*=4) reduction in the normalized relative protein expression of NCS-1 to β-actin, whereas the control dsRNA treatment did not affect the relative expression level of NCS-1 (2.7±2.5% reduction). (**C**,**D**) Confocal fluorescence images obtained from double immunocytochemical staining of β-actin and NCS-1, under different dsRNA treatments (5 nM) for 24 hours. (C) Representative β-actin and NCS-1 immunofluorescence images of PeA neurons in culture for 24 hours. (D) Summary of the NCS-1 levels from various regions of the culture PeA neurons. Relative fluorescence intensities of NCS to β-actin ratio (F_{NCS}/F_{Actin}) for the control dsRNA group: soma 1.48±0.08; neurite 1.51±0.12; branch point 1.44±0.05; and growth cone 1.60±0.12. The relative ratio for *NCS* dsRNA group: soma 0.84±0.06; neurite 0.94±0.13; branch point 0.97±0.08; growth cone 1.10±0.16. The data are presented as mean±s.e.m. and are obtained from a total of 10 control and 15 *NCS-1*-specific dsRNA-treated cells. Asterisk indicates significant difference (P<0.05) between the control and *NCS-1* dsRNA-treated conditions.

of new branches requires advancement of neurites, we opted to measure extension rates and retraction rates of individual neurites. During this period, the average rate of growth of individual neurites was 6.44±0.49 μm/hour (*n*=57) in the *NCS-1* dsRNA-treated neurons, 3.47±0.49 μm/hour (*n*=43) in the control dsRNA-treated neurons and 3.77±0.67 μm/hour in the mock group (Fig. 3C). This increase was significantly greater in the *NCS-1* dsRNA-treated neurons compared with that in the control dsRNA-treated neurons and mock group (P<0.05). The mean retraction rates varied from 0.76 to 1.16 μm/hour (mock control 1.17±0.46; control RNA 0.76±0.11; *NCS-1* RNA 0.95±0.16); the difference among the conditions, however, was not statistically significant (P>0.05). Our findings indicate that NCS-1 is involved in both neurite branching and extension processes in PeA neurons, and that a reduction of ~30% NCS-1 is sufficient to influence these processes.

NCS-1 knockdown reduces growth cone Ca^{2+} signals

Ca^{2+} homeostasis affects neurite outgrowth (Henley and Poo, 2004; Kater and Mills, 1991), so we examined whether NCS-1 modulates activity-dependent Ca^{2+} influx using ratiometric fura-2 calcium imaging. Activity was induced by somatic stimulation of 1 second current pulses via an intracellular sharp electrode. As expected, higher frequencies of action potentials (APs) resulted in higher peaks in $[Ca^{2+}]_i$, as shown by higher ratiometric fluorescent intensities (Fig. 4). The maximal fluorescent signal always coincided with the last spike of each action potential train, so we recorded and compared with the maximal signals under different conditions. The responsiveness of the *NCS-1* dsRNA-treated cells to APs was dramatically weaker than that of the mock or the control dsRNA-treated cells (Fig. 4A). We quantified the activity-dependency of the Ca^{2+} signal by plotting the maximal fura-2 ratiometric intensity ($F_{340/380}$) against the number of action potentials used to evoke the response (APs per second). As shown in Fig. 4B, the change in peak ratio intensity (evoked level–basal level) was linearly correlated to the number of action potentials at least up to 7 Hz. Summarized in Fig. 4C, *NCS-1* dsRNA-treated cells had a significantly lower degree of Ca^{2+} influx per action potential (0.010±0.004 AU/AP, *n*=5) than the control dsRNA (0.027±0.003 AU/AP, *n*=3) and mock treated cells (0.037±0.006, *n*=4). The measured basal Ca^{2+} levels, however, were similar between the treatments (AU; control 0.89±0.07; control dsRNA 0.86±0.04; *NCS-1* dsRNA 0.99±0.06; P>0.05). These results support the hypothesis that NCS-1 affects activity-dependent Ca^{2+} influx in growth cones.

The NCS-1 C-terminal peptide reduces growth cone Ca^{2+} current activities

The C-terminus of NCS-1 has been shown to regulate activity-dependent currents from presynaptic voltage-dependent Ca^{2+} channels (Tsujimoto et al., 2002). Assuming that NCS-1 modulates growth cone Ca^{2+} channels similarly, its effects on neurite outgrowth could be directly due to this modulation. To test this hypothesis, we

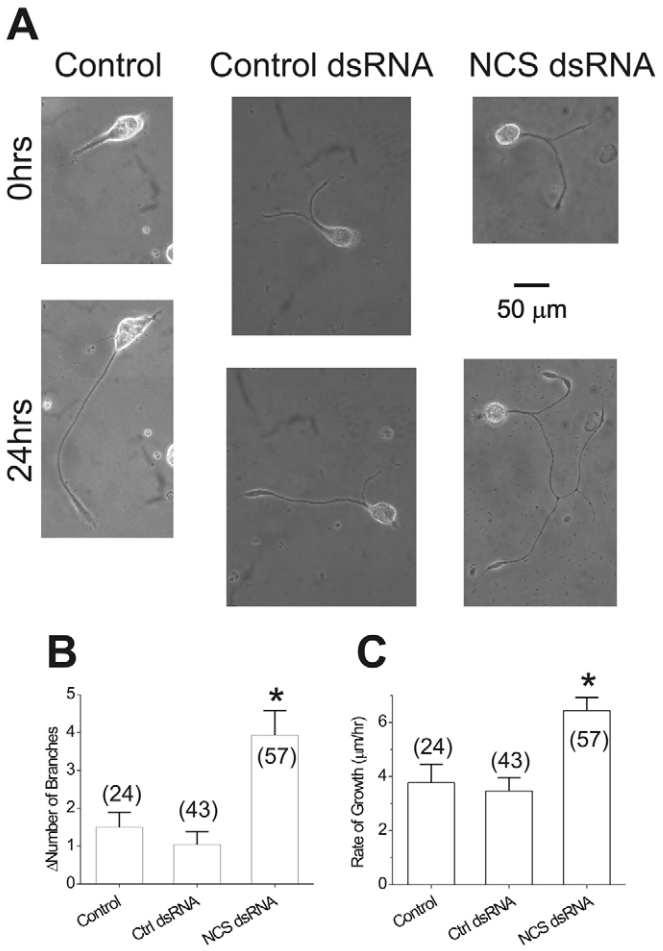

Fig. 3. NCS-1 knockdown enhances neurite outgrowth in *L. stagnalis*. (**A**) Phase-contrast images of a single PeA neuron before and 24 hours after addition of water (right), 5 nM control (middle) or *NCS-1*-specific (left) dsRNA. Cells were isolated and cultured in CM for 24 hours before treatment. (**B**,**C**) Neurite outgrowth was examined for the degree of branching (B) and the rate of extension (C). Both the number of new neurites (the degree of branching) and the rate of neurite extension were significantly higher after the *NCS-1*-specific dsRNA treatment compared with controls. The number of new neurites: mock control 1.50±0.39; control dsRNA (ctrl dsRNA) 1.04±0.39; and *NCS-1* dsRNA 3.93±0.65. The rate of the extension (μm/hour): mock control 3.77±0.67; control dsRNA 3.47±0.49; *NCS-1* dsRNA 6.44±0.49. The data are presented as mean±s.e.m. and obtained from 24 control, 43 control dsRNA and 57 *NCS-1*-specific dsRNA-treated cells. Asterisk indicates significant difference (P<0.05) from control condition.

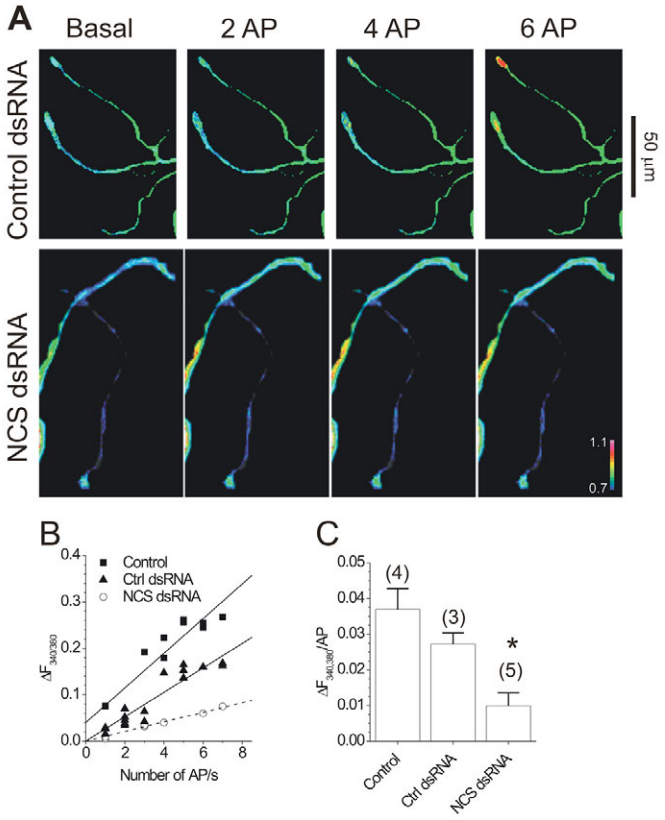

Fig. 4. NCS-1 knockdown affects the action potential-induced fura-2 Ca^{2+} signal in growth cones in an activity-dependent manner. (**A**) Representative epifluorescent images of Ca^{2+} signals in *L. stagnalis* neurites treated with the control dsRNA or *NCS-1* dsRNA. The Ca^{2+} ratiometric signals excited at 340 and 380 nm ($F_{340/380}$) were obtained at rest (basal) or elicited by two, four or six depolarization-induced action potentials. Action potentials were evoked by 1 second depolarization using an intracellular sharp electrode impaled into the soma. (**B**) Representative examples showing that the Ca^{2+} signal ($F_{340/380}$) was as a linear function of the number of action potentials. The Ca^{2+} signal from a single growth cone region was plotted against the number of action potentials used to evoke the response. The line represents a linear best fit of the data, which shows no apparent saturation of the signal within the range of action potentials used. The slopes of the fits are 0.037±0.004 (control), 0.031±0.003 (control dsRNA) or 0.011±0.001 (*NCS-1* dsRNA). The slope was used to quantify the dynamics of Ca^{2+} change resulting from action potential stimulation. (**C**) Summary of the slope of the fit described in B from three to five cells with treatments as indicated. The mean slope dependencies are 0.037±0.006 (control, n=4), 0.027±0.003 (control dsRNA, n=3), and 0.010±0.004 (*NCS-1* dsRNA, n=5). The data are presented as mean±s.e.m. Asterisk indicates significant difference (P<0.05) from the controls. AP, action potentials.

used a dominant-negative peptide to compete with C-terminal NCS-1 interactions (CTN) and examined its effects on three parameters: (1) voltage-dependent Ca^{2+} currents; (2) activity-dependent Ca^{2+} influx; and (3) neurite outgrowth properties.

We designed the CTN peptide to satisfy two criteria. First, the peptide should replicate the original study on C-terminal modulation of presynaptic Ca^{2+} channels (Tsujimoto et al., 2002). Second, it should be easily introduced into many cells. With these in mind, the peptide was made from the last 34 amino acids of the NCS-1 C-terminus, as in the previous study, linked at its N-terminus by a tetra-glycine spacer to the HIV-TAT protein transduction domain sequence (see Fig. S1A in the supplementary material), which allows it to readily translocate across cell membranes (Vives et al., 1997). A scrambled control peptide (srCTN) was similarly synthesized (see Materials and methods). Using a BODIPY-tagged CTN, we found that 5 minute incubation with *L. stagnalis* PeA neurons was enough to allow for the fluorescent signal to invade the cytosol (see Fig. S1B in the supplementary material), showing that a short exposure was sufficient for CTN to access the intracellular space of the neurons. This is consistent with previous

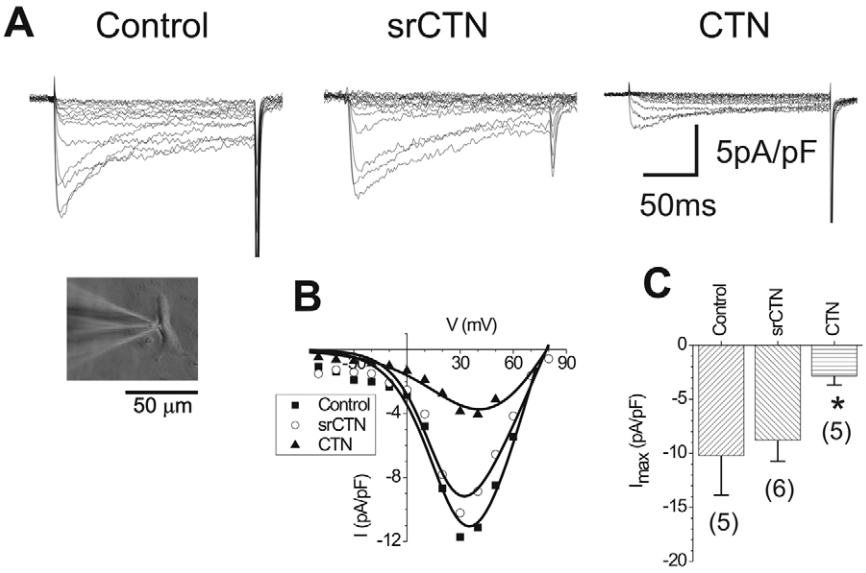

Fig. 5. CTN reduces Ca^{2+} currents from growth cones of isolated PeA neurons in *L. stagnalis*. (**A**) Representative Ca^{2+} (ruptured) whole-cell currents from a single transected growth cone (including adjacent neurite) without or with 50 μM scrambled CTN (srCTN) or CTN treatment. The currents were evoked from a holding potential of –100 mV and stepped from –60 mV to +80 mV at 10 mV increments, using a P/4 protocol. Currents were normalized by capacitance (pF). A phase-contrast imaging of a transected growth cone is shown in the insert at the bottom left. (**B**) Current density-voltage (I-V) plots from the traces in A. Peak current densities are smaller after CTN treatment compared to srCTN treatment and control conditions. The line represents a modified Boltzmann fit of the data, as described in Materials and methods and listed as G(pS/pF), Vrev (mV) and Vh (mV): control 0.34, 79 and 23; srCTN 0.27, 78 and 20; CTN 0.18, 80 and 40, respectively. (**C**) Average peak current density suggests that CTN significantly (P<0.05) reduces the peak current density in growth cones of PeA neurons. Data were obtained from five control (10.3±3.0 pA/pF), six srCTN (9.0±1.3 pA/pF) and five CTN (2.1±0.9 pA/pF) experiments. The data are presented as mean±s.e.m. Asterisk indicates significant difference (P<0.05) from the control condition.

reports of rapid uptake of TAT and other protein-transduction-domain-tagged peptides (Dunican and Doherty, 2001; Green et al., 2003). The distribution of the labelled CTN appeared to be Gaussian along the z-axis for somata, neurites and growth cones (see Fig. S1C in the supplementary material) and only excluded from the nucleus, similar to a previous study (Vocero-Akbani et al., 2000) that showed that TAT-linked peptides have relatively uniform access to all compartments of the cell without any strong specificity for any particular organelle or membrane.

Having shown that CTN sufficiently invades the cell, we examined its effects on voltage-dependent Ca^{2+} currents in growth cones. Currents were recorded for either transected growth cones that were untreated or treated for at least 5 minutes with either 50 μM CTN or srCTN. Representative records of Ca^{2+} currents from a transected growth cone (Fig. 5, insert) and the I-V plots of the current under different treatments are shown in Fig. 5A, and Fig. 5B, respectively. The activity peaked rapidly upon depolarization and decayed slowly to a sustained level over the course of the 200 millisecond step, which is typical of currents from high voltage-activated Ca^{2+} channels. As the size of the growth cones varied between preparations, we normalized the peak current amplitude with the cell size (pF) to compare current densities. The maximal current density was significantly reduced by CTN (2.9±0.8 pA/pF) compared with the controls (untreated 10.2±3.6 pA/pF; srCTN 8.9±2.0 pA/pF), both of which were similar (Fig. 5B). In some experiments, the peptide was also added to the patch pipette solution with similar results, suggesting that the findings were not due to dialysis of the cytosol. Aside from the density, the general profile of the Ca^{2+} I-V plots was not affected by CTN. Thus, in addition to presynaptic Ca^{2+} channels, CTN also suppresses growth cone Ca^{2+} channel activity. Consequently, NCS-1 appears to regulate growth cone Ca^{2+} channels through interactions of its C-terminus.

The NCS-1 C-terminal peptide decreases activity-dependent Ca^{2+} dynamics in growth cones

We have shown that NCS-1 knockdown reduces intracellular Ca^{2+} influx and a peptide of its C-terminus reduces voltage-dependent Ca^{2+} currents. Consequently, we asked whether the RNA interference effects were mimicked by the C-terminal peptide. We examined the acute effects of 50 μM CTN (or srCTN) on activity-dependent Ca^{2+} signals in growth cones of PeA cells. After the peptide was added to the bath, 5 minutes were allotted before recording to ensure that the peptide was in the cells. In some cases, the activity-dependent Ca^{2+} signalling was recorded before peptide treatment to allow for paired assessment of the changes, avoiding any cell-specific differences. Fig. 6A shows representative Ca^{2+} signals in the neurites of a sprouted PeA cell in response to one, three or six action potentials before and after CTN treatment. As with the dsRNA treatments, the changes in fluorescence intensity ratio ($F_{340/380}$) in growth cones exhibited a positive linear relationship with the number of action potentials for up to 7 Hz (Fig. 6B). After the CTN-treatment (0.019±0.002 AU/AP) this correlation was reduced compared with control (0.037±0.004 AU/AP), whereas srCTN-treatment did not appear to affect it (0.041±0.002 AU/AP). Comparing these slopes from several independent experiments (Fig. 6C), the activity-dependent Ca^{2+} influx in control (untreated) cells (0.037±0.006 AU/AP; n=4) was significantly reduced by CTN (0.021±0.003 AU/AP; n=8; P<0.05), but not by srCTN (0.042±0.004 AU/AP, n=3), indicating that NCS-1 affects activity-dependent Ca^{2+} influx in these regions. The basal Ca^{2+} level under resting conditions was not significantly affected by the peptide (control 0.89±0.07 AU; CTN 0.98±0.06 AU; srCTN 0.88±0.09 AU). Our findings indicate that the C-terminus of NCS-1 is at least partly responsible for regulating activity-dependent Ca^{2+}-dynamics in growth cones.

Compared with the reduction in activity-dependent Ca^{2+} influx caused by *NCS-1* knockdown (0.010±0.004 AU/AP), CTN appeared less effective (0.021±0.003 AU/AP). We next examined the role of CTN on neurite behaviour and asked whether CTN may mimic the dsRNA effects on neurite extension and branching.

C-terminus of NCS-1 affects neurite branching

We have shown that, similar to *NCS-1* RNA knockdown, the NCS-1 C-terminus interactions affected activity-dependent Ca^{2+} influx and voltage-dependent Ca^{2+} currents (Figs 5 and 6). We next examined whether the NCS-1 C-terminus interactions are

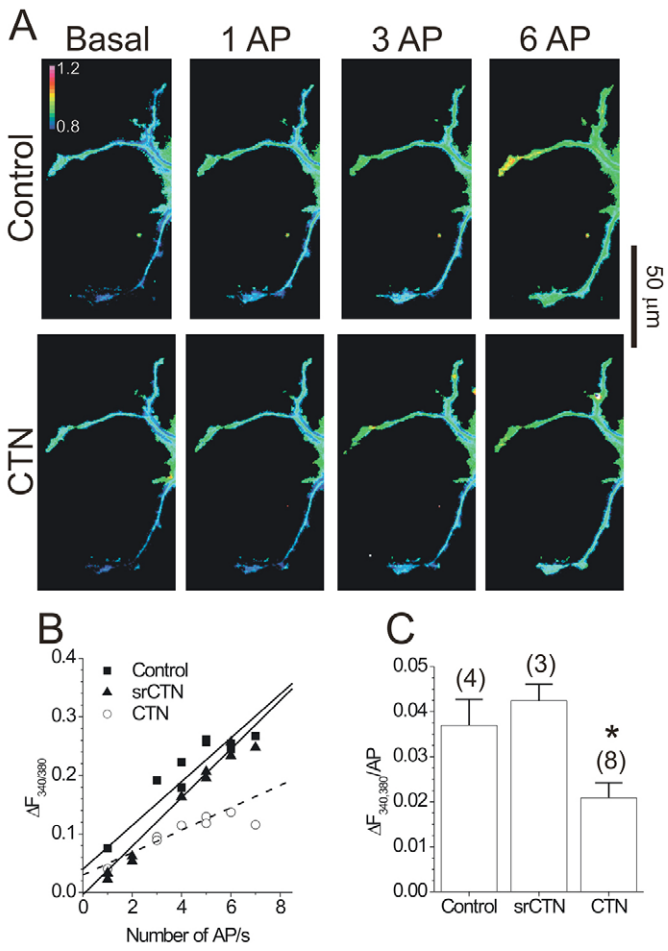

Fig. 6. The C-terminus of NCS-1 peptide (CTN) affects the action potential-induced fura-2 Ca^{2+} signal in growth cones in an activity-dependent manner. (**A**) Representative epifluorescent images of Ca^{2+} signals in *L. stagnalis* neurites before (control) and after CTN treatment (50 μM). The Ca^{2+} ratiometric signals ($F_{340/380}$) were obtained at rest (basal) or elicited by one, four or six depolarization-induced action potentials. Action potentials were evoked by 1 second depolarization using an intracellular sharp electrode impaled into the soma. (**B**) Representative examples showing the Ca^{2+} signal ($F_{340/380}$) were as a linear function of the number of action potentials in the neurites under different conditions. The Ca^{2+} signal from a single growth cone region was plotted against the number of action potentials used to evoke the response. The line represents a linear best fit of the data, which shows no apparent saturation of the signal within the range of action potentials used. The slopes of the plots are 0.037±0.004 (control), 0.041±0.002 (srCTN) and 0.019±0.002 (CTN). (**C**) Summary of the slope, as described in B, from three to eight cells with treatments as indicated. The mean slope dependencies are 0.037±0.006 (control, *n*=4), 0.042±0.004 (srCTN, *n*=3) and 0.021±0.003 (CTN, *n*=8). The data are presented as mean±s.e.m. Asterisk indicates significant difference (*P*<0.05) from the controls. AP, action potentials.

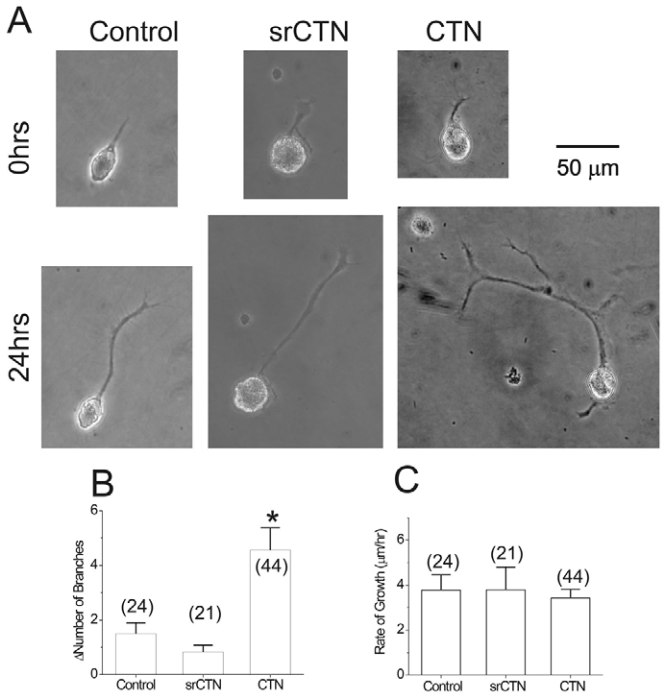

Fig. 7. CTN increases the rate of neurite branching but not of neurite growth in *L. stagnalis*. (**A**) Phase-contrast images of a single PeA neuron before and 24 hours after treatment with water (control, left), 50 μM srCTN (middle) or 50 μM CTN (right). Cells were isolated and cultured in CM 24 hours before treatment. (**B**,**C**) Neurite branching but not the rate of neurite extension was selectively affected by CTN treatment. (B) Branching (as indicated by the number of new neurites) increased in CTN-treated cells as soon as 3 hours after treatment (mock control 1.50±0.39; srCTN 0.83±0.25; CTN 4.57±0.81). (C) The rate of the neurite extension did not differ between the treatments (mock control 3.77±0.67 μm/hour; srCTN 3.79±1.02 μm/hour; CTN 3.43±0.38 μm/hour). The data are presented as mean±s.e.m. and were obtained from 24 control, 21 srCTN and 44 CTN cells. Asterisk indicates significant difference (*P*<0.05) from control condition.

responsible for the effects of NCS-1 knockdown on neurite outgrowth. As in the dsRNA experiments, CTN was added to PeA neurons 24 hours after plating the cells, and the change in outgrowth was examined 24 hours later. Again, ~80% of neurites advanced and the remaining neurites either retracted or remained unchanged during the period of treatment (24 hours). From cells that started with similar degrees of growth (Fig. 7A, 0 hours), CTN-treated cells showed more elaborate branching 24 hours after treatment than did the controls. On average, there were significantly more new branches in CTN-treated neurons (4.57±0.81, *n*=44) compared with mock (1.50±0.39, *n*=24) and srCTN-treated neurons (0.83±0.25, *n*=21) (Fig. 7B, *P*<0.05). Treatment of srCTN had no significant effect compared to mock. The degree of neurite branching in CTN-treated cells was similar to that in NCS-1 dsRNA-treated cells (Fig. 3B), supporting the idea that the C-terminus of NCS-1 may be involved in neurite branching.

In contrast to branching, CTN did not affect neurite extension to the same degree as NCS-1 knockdown. The extension rate of CTN-treated neurites (3.43±0.38 μm/hour) was similar to that in the mock control (3.77±1.67 μm/hour) and srCTN-treatment (3.79±1.02 μm/hour). Similarly, no significant difference was observed in the retraction rates from the three groups (mock control 1.17±0.46; srCTN 1.8±0.48; CTN 0.93±0.22; *P*>0.05). However, dsRNA-treated neurons (6.44±0.49 μm/hour) grew twice as fast as untreated neurons (3.77±0.67 μm/hour). These findings suggest that the involvement of NCS-1 in neurite extension does not require C-terminal interactions that are competed with by CTN.

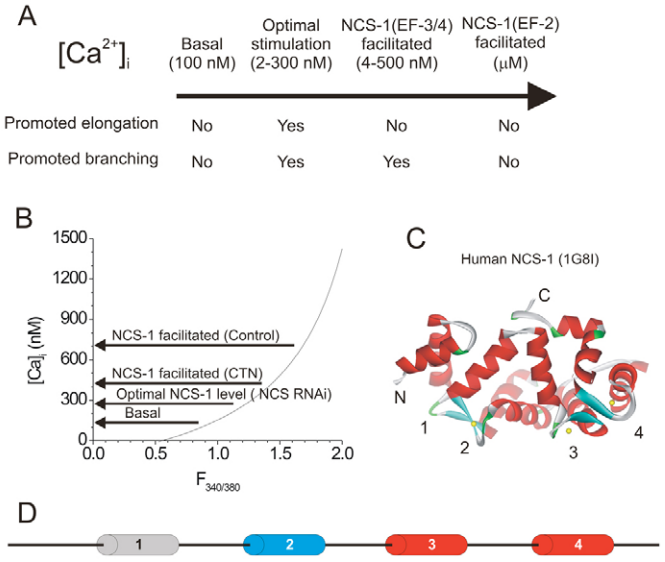

Fig. 8. Model of NCS-1 in Ca^{2+}-dependent neurite outgrowth pattern in *L. stagnalis*. (**A**) Neurite outgrowth processes, elongation and branching, are dependent on $[Ca^{2+}]_i$. At basal Ca^{2+} (~100 nM), both processes are negligible (Stage 1). Optimal electrical or chemical stimulation increases $[Ca^{2+}]_i$ (200-300 nM) and causes both process to be activated (Stage 2). This level of Ca^{2+} would be sufficient to allow binding to the high-affinity sites in NCS-1, thus allowing further Ca^{2+} increases (400-500 nM) through a positive-feedback mechanism such as NCS-1 stimulation of TRPC5 (Stage 3). At this stage, neurite extension is inhibited without affecting branching; but as the morphological determination of branching cannot be observed without extension, the branching also appears stalled. If the levels of Ca^{2+} continue to elevate (micromolar quantities), the likelihood of binding to the low-affinity site in NCS-1 is increased, thereby facilitating voltage-dependent Ca^{2+} channels and consequently raising the levels higher (Stage 4). At this stage, neurite outgrowth processes are both limited. (**B**) Calibration curve of Fura-2 signal against free $[Ca^{2+}]_i$. From the Ca^{2+}-imaging data (Figs 4 and 6), a calibration curve was constructed as described previously (Feng et al., 2002; Grynkiewicz et al., 1985). The arrows indicate the Ca^{2+} levels in PeA cells at either resting (basal) or electrically stimulated conditions with different treatments, and their corresponding stages as described in the model. (**C**,**D**) Structure of NCS-1 protein. (C) Tertiary structure of human NCS-1 (also known as FREQ – HUGO) protein (1G8I). Indicated are the N- and C-termini as well as the four EF-hand structures. Ca^{2+} ions are shown as yellow spheres bound to the three functional EF-hands. (D) Schematic structure of the protein showing the four EF-hands is shown below. Of the EF-hands, three are functional (coloured) and one is non-functional (grey). The high-affinity Ca^{2+}-binding sites (red), EF3 and EF4, are adjacent to each other and the C-terminus. Binding of Ca^{2+} to EF3 and the low-affinity site EF2 (blue) exposes a hydrophobic crevasse and putative binding pocket for interacting proteins (Bourne et al., 2001).

Our findings are unlikely to be the result of differences in the effectiveness of delivery and efficacy between dsRNA and peptide treatments. In particular, the rates of extension and degrees of branching were measured from the same cells, even though they are differentially modulated by CTN compared with *NCS-1* knockdown. These results indicate that NCS-1 affects neurite outgrowth at the level of both neurite extension and elaboration, and that C-terminal interactions are mostly involved in regulating neurite branching. Thus, distinct regions of NCS-1 appear to be differentially responsible for regulating the rate of neurite extension and the degree of neurite branching.

DISCUSSION

Neurite outgrowth depends on the level of intracellular Ca^{2+} (see Gomez and Spitzer, 2000; Henley and Poo, 2004; Kater and Mills, 1991). Too little Ca^{2+} and the neurites do not grow; too much Ca^{2+} and the growth stalls. An optimal window level of Ca^{2+} may be necessary for neurite outgrowth (Kater and Mills, 1991). Many sources of Ca^{2+} have been well studied and their regulation well established (Berridge et al., 2003), but to our knowledge there have been no studies on how the window level of Ca^{2+} is achieved and what molecules are involved. Here we report that NCS-1 regulates neurite outgrowth by modulating the local Ca^{2+} concentration to at least two different stimulated levels: the higher level affects neurite branching only, and the lower level affects both branching and extension. Our findings suggest that there are at least two distinct regions on NCS-1 that function independently to regulate the level of cytosolic Ca^{2+} levels, thereby modulating neurite outgrowth.

Ca^{2+} is an important regulator of neurite extension and growth cone pathfinding (Gomez and Spitzer, 2000). Intracellular Ca^{2+} transients can modulate the rate of neuronal migration in cerebellar microexplant cultures (Komuro and Rakic, 1996) and cortical cultures (Tang et al., 2003), and can also induce growth cone turning in cultured *Xenopus* neurons (Zheng, 2000). Neurite branching is also an activity-dependent event (see Dent et al., 2003). Inhibiting neuronal activity or blocking Ca^{2+}-conducting channels such as the AMPA (Uesaka et al., 2005) or NMDA (Ruthazer et al., 2003) receptors suppresses branching; and repetitive Ca^{2+} transients induced by netrin-1 facilitated release of intracellular Ca^{2+} stores promotes branching (Tang and Kalil, 2005). In parallel with these findings, we show that NCS-1 affects both neurite outgrowth and activity-dependent Ca^{2+} influx at the growth cones.

One target of NCS-1 was recently found by others to be a canonical TRP channel, TRPC5 (Hui et al., 2006). When overexpressing the dominant-negative NCS-1 mutant E120Q in PC12 cells, the Ca^{2+} influx through TRPC5 was reduced and the rate of neurite extension was enhanced, but branching was unchanged. There are some similarities between these findings to ours. First, we found that dsRNA knockdown of *NCS-1* expression in *L. stagnalis* neurons increased the rate of neurite extension. Second, in both *NCS-1* knockdown and CTN treatment, the activity-dependent Ca^{2+} influx was suppressed compared with untreated cells. In contrast to the NCS-1 E120Q mutant study, we found that NCS-1 is also involved in neurite branching via its C-terminus. We believe that this discrepancy lies in the use of different experimental tools. The mutation in E120Q abolishes the third NCS-1 EF-hand motif (EF-3), which is required for Ca^{2+}-dependent conformational changes, leaving other EF-hands and functional domains intact (Weiss et al., 2000). NCS-1 knockdown encompasses these effects, as it reduces the expression level of the protein; but CTN competes with the C-terminus interactions and may not affect EF-3 interactions. Thus, NCS-1 has two distinct effects on neurite outgrowth properties that are mediated by different structural domains of NCS-1: one involving EF-3 and another involving the C-terminus.

NCS-1 contains four EF-hand Ca^{2+}-binding motifs and can coordinate three Ca^{2+} ions when saturated (Fig. 8C,D) (Ames et al., 2000). The first N-terminal EF-hand (EF-1) is non-functional (Cox et al., 1994); the second EF-hand (EF-2) binds Ca^{2+} with a relatively low affinity (Kd: 10 μM) compared with the third (EF-3) and fourth (EF-4) EF-hands (Kd: 400 nM) (Ames et al., 2000). Mutation of EF-3 (E120Q) upregulates non-L-type Ca^{2+} channels in chromaffin cells (Weiss et al., 2000), and, as mentioned above, suppresses TRPC5 channels in PC12 cells (Hui et al., 2006). These opposing effects of

E120Q may arise from interactions on other regions of NCS-1. For example, the C-terminus encompassing part of EF-4 is involved in activity-dependent facilitation of the presynaptic P/Q type Ca^{2+} channels in the Calyx of Held (Tsujimoto et al., 2002). Although Ca^{2+} binding to the EF-hands in NCS-1 may be highly cooperative (Ames et al., 2000), these studies suggest that the different regions of NCS-1 can function independently of each other.

The binding affinities of the EF-hands in NCS-1 appear to be compatible with the optimal window level of Ca^{2+} that permits neurite outgrowth (Kater and Mills, 1991). In both mammalian (Connor, 1986) and invertebrate cultured neurons (Cohan et al., 1987), intracellular Ca^{2+} concentrations of 40-80 nM produce stable growth cones; 100-300 nM Ca^{2+} concentrations induce neurite outgrowth; and higher levels retard growth (Kater et al., 1989). Domains EF-3 and EF-4 in NCS-1 have Ca^{2+}-binding affinities around 400 nM, just above the concentration threshold that is necessary for optimal neurite outgrowth; and EF-2 has a binding affinity around 10 μM, which lies in the range of outgrowth inhibition (Ames et al., 2000). Consequently, NCS-1 appears to have suitable structural features to respond to levels of intracellular Ca^{2+} around the optimal window necessary for neurite outgrowth.

Based on our findings, we envision a four-stage mechanism where NCS-1 is involved in activity-dependent neurite outgrowth (Fig. 8). First, at basal levels of Ca^{2+}, NCS-1 may or may not be involved in limited outgrowth. Second, an optimal range of neuronal activity evokes Ca^{2+} influx (200–300 nM) to promote both neurite extension and branching. Higher activity, leading to higher Ca^{2+} influx, may inhibit both processes through an NCS-1-dependent mechanism, as described in stages three and four. Third, increasing Ca^{2+} allows it to bind to one or more of the high-affinity sites on NCS-1, consequently inhibiting elongation while still promoting branching. The elevation in Ca^{2+} in this stage may be partly due to NCS-1 facilitation of TRPC5 channels (Hui et al., 2006). Fourth, raising Ca^{2+} to higher levels allows it to bind to the low-affinity site on NCS-1 and also inhibit branching. The Ca^{2+} source at this stage may involve NCS-1 facilitation of growth cone voltage-dependent Ca^{2+} channels, leading to a positive-feedback mechanism to limit outgrowth until the stimulus is relaxed (i.e. Ca^{2+} levels fall to, and below that, of stage three). In this manner, branching and subsequent extension could be controlled by an NCS-1-dependent mechanism involving dynamic changes in the intracellular Ca^{2+} level. This simple model emphasizes that different windows of $[Ca^{2+}]_i$ are permissive for neurite extension and branching, with NCS-1 modulating both processes in a $[Ca^{2+}]_i$-dependent manner.

The individual stages of our model of NCS-1-dependent outgrowth can be attributed to different regions of the protein. The third EF-hand (EF-3) was previously shown to be selectively involved in neurite extension (Hui et al., 2006). Disrupting this Ca^{2+}-binding site, as in the E120Q mutant, prevented NCS-1 inhibition of neurite extension in stage three of the model without affecting stage four: branching remained unaffected. In the current study, we show that the C-terminus is selectively involved in neurite branching. Competing with NCS-1 C-terminal interactions via the CTN peptide alleviated inhibition of branching in stage four without affecting stage three: neurite extension remained impeded. We show that NCS-1 is responsible for both effects, as knockdown by RNA interference affected both stages three and four, consequently preventing suppression of both branching and extension. As with other functional properties of this protein (Burgoyne et al., 2004), the different domains in NCS-1 appear to act independently in its modulation of neurite outgrowth, with the third EF-hand responsible for extension and the C-terminus responsible for branching.

The mechanism underlying neurite branching remains unclear but is thought to be an activity-dependent event (Tang et al., 2003; Zheng, 2000) (see also Dent et al., 2003). Our study suggests that NCS-1 is involved perhaps by fine-tuning local Ca^{2+} transients. It is the spatial localization of Ca^{2+} transients that determines the pathway of axonal development. In particular, Ca^{2+} transients in the growth cone stimulate axon extension (Gu and Spitzer, 1995) and Ca^{2+} transients in the filopodia induce growth cone turning (Gomez et al., 2001). The downstream actions of Ca^{2+} in neurons include control of growth cone traction (Conklin et al., 2005), polymerization of cytoskeletal structural elements (Lautermilch and Spitzer, 2000) and membrane insertion at growth cones (Lockerbie et al., 1991; Wood et al., 1992), which have direct effects on neurite outgrowth behaviour. By creating local increases in $[Ca^{2+}]_i$ at growth cones, the neurite can be steered (Henley and Poo, 2004). Consequently, the ability of NCS-1 to modulate Ca^{2+} dynamics at developing growth cones endows it the ability to regulate neurite outgrowth.

In conclusion, we showed that by modulating different levels of cytosolic Ca^{2+}, NCS-1 can influence neurite outgrowth properties. NCS-1 not only facilitates the functioning of the fully mature synapse, but it is also crucial during the conception of the synapse by modulation of Ca^{2+} dynamics, and neurite extension and branching.

This work was supported by an operating grant to Z.-P.F. from the Canadian Institutes of Health Research (CIHR MOP 62738), start-up funds from the Department of Physiology, the Faculty of Medicine and the University of Toronto, and equipment grants from Canada Foundation for Innovation (CFI) and Ontario Innovation Trust (OIT). B.J.S. holds a Doctoral Research Award from the CIHR and fellowships from the Bank of Montreal, the James F. Crothers Foundation and the Margaret and Howard Gamble Foundation. J.C.C.R. holds a Canada Research Chair in Learning and Memory, Tier I. Z.-P.F. holds a New Investigator Award from the CIHR, a Premier's Research Excellence Award of Ontario and a Young Investigator Award from Boehringer Ingelheim (Canada).

Supplementary material

Supplementary material for this article is available at http://dev.biologists.org/cgi/content/full/134/24/4479/DC1

References

Ames, J. B., Porumb, T., Tanaka, T., Ikura, M. and Stryer, L. (1995). Amino-terminal myristoylation induces cooperative calcium binding to recoverin. *J. Biol. Chem.* **270**, 4526-4533.

Ames, J. B., Ishima, R., Tanaka, T., Gordon, J. I., Stryer, L. and Ikura, M. (1997). Molecular mechanics of calcium-myristoyl switches. *Nature* **389**, 198-202.

Ames, J. B., Hendricks, K. B., Strahl, T., Huttner, I. G., Hamasaki, N. and Thorner, J. (2000). Structure and calcium-binding properties of Frq1, a novel calcium sensor in the yeast Saccharomyces cerevisiae. *Biochemistry* **39**, 12149-12161.

Angaut-Petit, D., Toth, P., Rogero, O., Faille, L., Tejedor, F. J. and Ferrus, A. (1998). Enhanced neurotransmitter release is associated with reduction of neuronal branching in a Drosophila mutant overexpressing frequenin. *Eur. J. Neurosci.* **10**, 423-434.

Berridge, M. J., Bootman, M. D. and Roderick, H. L. (2003). Calcium signalling: dynamics, homeostasis and remodelling. *Nat. Rev. Mol. Cell Biol.* **4**, 517-529.

Bourne, Y., Dannenberg, J., Pollmann, V., Marchot, P. and Pongs, O. (2001). Immunocytochemical localization and crystal structure of human frequenin (neuronal calcium sensor 1). *J. Biol. Chem.* **276**, 11949-11955.

Burgoyne, D. (2004). The neuronal calcium-sensor proteins. *Biochim. Biophys. Acta* **1742**, 59-68.

Burgoyne, R. D. (2007). Neuronal calcium sensor proteins: generating diversity in neuronal Ca(2+) signalling. *Nat. Rev. Neurosci.* **8**, 182-193.

Burgoyne, R. D., O'Callaghan, D. W., Hasdemir, B., Haynes, L. P. and Tepikin, A. V. (2004). Neuronal Ca2+-sensor proteins: multitalented regulators of neuronal function. *Trends Neurosci.* **27**, 203-209.

Chen, X. L., Zhong, Z. G., Yokoyama, S., Bark, C., Meister, B., Berggren, P. O., Roder, J., Higashida, H. and Jeromin, A. (2001). Overexpression of rat neuronal calcium sensor-1 in rodent NG108-15 cells enhances synapse formation and transmission. *J. Physiol.* **532**, 649-659.

Cohan, C. S., Connor, J. A. and Kater, S. B. (1987). Electrically and chemically mediated increases in intracellular calcium in neuronal growth cones. *J. Neurosci.* **7**, 3588-3599.
Conklin, M. W., Lin, M. S. and Spitzer, N. C. (2005). Local calcium transients contribute to disappearance of pFAK, focal complex removal and deadhesion of neuronal growth cones and fibroblasts. *Dev. Biol.* **287**, 201-212.
Connor, J. A. (1986). Digital imaging of free calcium changes and of spatial gradients in growing processes in single, mammalian central nervous system cells. *Proc. Natl. Acad. Sci. USA* **83**, 6179-6183.
Cox, J. A., Durussel, I., Comte, M., Nef, S., Nef, P., Lenz, S. E. and Gundelfinger, E. D. (1994). Cation binding and conformational changes in VILIP and NCS-1, two neuron-specific calcium-binding proteins. *J. Biol. Chem.* **269**, 32807-32813.
Dent, E. W., Tang, F. and Kalil, K. (2003). Axon guidance by growth cones and branches: common cytoskeletal and signaling mechanisms. *Neuroscientist* **9**, 343-353.
Dunican, D. J. and Doherty, P. (2001). Designing cell-permeant phosphopeptides to modulate intracellular signaling pathways. *Biopolymers* **60**, 45-60.
Dyer, J. R., Sossin, W. S. and Klein, M. (1996). Cloning and characterization of aplycalcin and Aplysia neurocalcin, two new members of the calmodulin superfamily of small calcium-binding proteins. *J. Neurochem.* **67**, 932-942.
Feng, Z. P., Klumperman, J., Lukowiak, K. and Syed, N. I. (1997). In vitro synaptogenesis between the somata of identified Lymnaea neurons requires protein synthesis but not extrinsic growth factors or substrate adhesion molecules. *J. Neurosci.* **17**, 7839-7849.
Feng, Z. P., Grigoriev, N., Munno, D., Lukowiak, K., MacVicar, B. A., Goldberg, J. I. and Syed, N. I. (2002). Development of Ca2+ hotspots between Lymnaea neurons during synaptogenesis. *J. Physiol.* **539**, 53-65.
Gomez, T. M. and Spitzer, N. C. (2000). Regulation of growth cone behavior by calcium: new dynamics to earlier perspectives. *J. Neurobiol.* **44**, 174-183.
Gomez, T. M., Robles, E., Poo, M. and Spitzer, N. C. (2001). Filopodial calcium transients promote substrate-dependent growth cone turning. *Science* **291**, 1983-1987.
Green, I., Christison, R., Voyce, C. J., Bundell, K. R. and Lindsay, M. A. (2003). Protein transduction domains: are they delivering? *Trends Pharmacol. Sci.* **24**, 213-215.
Grynkiewicz, G., Poenie, M. and Tsien, R. Y. (1985). A new generation of Ca2+ indicators with greatly improved fluorescence properties. *J. Biol. Chem.* **260**, 3440-3450.
Gu, X. and Spitzer, N. C. (1995). Distinct aspects of neuronal differentiation encoded by frequency of spontaneous Ca2+ transients. *Nature* **375**, 784-787.
Guo, W., Malin, S. A., Johns, D. C., Jeromin, A. and Nerbonne, J. M. (2002). Modulation of Kv4-encoded K(+) currents in the mammalian myocardium by neuronal calcium sensor-1. *J. Biol. Chem.* **277**, 26436-26443.
Henley, J. and Poo, M. M. (2004). Guiding neuronal growth cones using Ca2+ signals. *Trends Cell Biol.* **14**, 320-330.
Hui, H., McHugh, D., Hannan, M., Zeng, F., Xu, S. Z., Khan, S. U., Levenson, R., Beech, D. J. and Weiss, J. L. (2006). Calcium-sensing mechanism in TRPC5 channels contributing to retardation of neurite outgrowth. *J. Physiol.* **572**, 165-172.
Hui, K., Guo, Y. and Feng, Z. P. (2005). Biophysical properties of menthol-activated cold receptor TRPM8 channels. *Biochem. Biophys. Res. Commun.* **333**, 374-382.
Kabbani, N., Negyessy, L., Lin, R., Goldman-Rakic, P. and Levenson, R. (2002). Interaction with neuronal calcium sensor NCS-1 mediates desensitization of the D2 dopamine receptor. *J. Neurosci.* **22**, 8476-8486.
Kapp-Barnea, Y., Melnikov, S., Shefler, I., Jeromin, A. and Sagi-Eisenberg, R. (2003). Neuronal calcium sensor-1 and phosphatidylinositol 4-kinase beta regulate IgE receptor-triggered exocytosis in cultured mast cells. *J. Immunol.* **171**, 5320-5327.
Kater, S. B. and Mills, L. R. (1991). Regulation of growth cone behavior by calcium. *J. Neurosci.* **11**, 891-899.
Kater, S. B., Mattson, M. P. and Guthrie, P. B. (1989). Calcium-induced neuronal degeneration: a normal growth cone regulating signal gone awry (?). *Ann. N. Y. Acad. Sci.* **568**, 252-261.
Kawasaki, T., Nishio, T., Kurosawa, H., Roder, J. and Jeromin, A. (2003). Spatiotemporal distribution of neuronal calcium sensor-1 in the developing rat spinal cord. *J. Comp. Neurol.* **460**, 465-475.
Kim, D. H., Behlke, M. A., Rose, S. D., Chang, M. S., Choi, S. and Rossi, J. J. (2005). Synthetic dsRNA Dicer substrates enhance RNAi potency and efficacy. *Nat. Biotechnol.* **23**, 222-226.
Komuro, H. and Rakic, P. (1996). Intracellular Ca2+ fluctuations modulate the rate of neuronal migration. *Neuron* **17**, 275-285.
Lautermilch, N. J. and Spitzer, N. C. (2000). Regulation of calcineurin by growth cone calcium waves controls neurite extension. *J. Neurosci.* **20**, 315-325.
Lockerbie, R. O., Miller, V. E. and Pfenninger, K. H. (1991). Regulated plasmalemmal expansion in nerve growth cones. *J. Cell Biol.* **112**, 1215-1227.
Nakamura, T. Y., Pountney, D. J., Ozaita, A., Nandi, S., Ueda, S., Rudy, B. and Coetzee, W. A. (2001). A role for frequenin, a Ca2+-binding protein, as a regulator of Kv4 K+-currents. *Proc. Natl. Acad. Sci. USA* **98**, 12808-12813.
O'Callaghan, D. W., Ivings, L., Weiss, J. L., Ashby, M. C., Tepikin, A. V. and Burgoyne, R. D. (2002). Differential use of myristoyl groups on neuronal calcium sensor proteins as a determinant of spatio-temporal aspects of Ca2+ signal transduction. *J. Biol. Chem.* **277**, 14227-14237.
Rousset, M., Cens, T., Gavarini, S., Jeromin, A. and Charnet, P. (2003). Down-regulation of voltage-gated Ca2+ channels by neuronal calcium sensor-1 is beta subunit-specific. *J. Biol. Chem.* **278**, 7019-7026.
Ruthazer, E. S., Akerman, C. J. and Cline, H. T. (2003). Control of axon branch dynamics by correlated activity in vivo. *Science* **301**, 66-70.
Schaad, N. C., de Castro, E., Nef, S., Hegi, S., Hinrichsen, R., Martone, M. E., Ellisman, M. H., Sikkink, R., Rusnak, F., Sygush, J. et al. (1996). Direct modulation of calmodulin targets by the neuronal calcium sensor NCS-1. *Proc. Natl. Acad. Sci. USA* **93**, 9253-9258.
Schlecker, C., Boehmerle, W., Jeromin, A., DeGray, B., Varshney, A., Sharma, Y., Szigeti-Buck, K. and Ehrlich, B. E. (2006). Neuronal calcium sensor-1 enhancement of InsP3 receptor activity is inhibited by therapeutic levels of lithium. *J. Clin. Invest.* **116**, 1668-1674.
Spencer, G. E., Syed, N. I., Lukowiak, K. and Winlow, W. (1995). Halothane-induced synaptic depression at both in vivo and in vitro reconstructed synapses between identified Lymnaea neurons. *J. Neurophysiol.* **74**, 2604-2613.
Syed, N. I., Bulloch, A. G. and Lukowiak, K. (1990). In vitro reconstruction of the respiratory central pattern generator of the mollusk Lymnaea. *Science* **250**, 282-285.
Tanaka, T., Ames, J. B., Harvey, T. S., Stryer, L. and Ikura, M. (1995). Sequestration of the membrane-targeting myristoyl group of recoverin in the calcium-free state. *Nature* **376**, 444-447.
Tang, F. and Kalil, K. (2005). Netrin-1 induces axon branching in developing cortical neurons by frequency-dependent calcium signaling pathways. *J. Neurosci.* **25**, 6702-6715.
Tang, F., Dent, E. W. and Kalil, K. (2003). Spontaneous calcium transients in developing cortical neurons regulate axon outgrowth. *J. Neurosci.* **23**, 927-936.
Taverna, E., Francolini, M., Jeromin, A., Hilfiker, S., Roder, J. and Rosa, P. (2002). Neuronal calcium sensor 1 and phosphatidylinositol 4-OH kinase beta interact in neuronal cells and are translocated to membranes during nucleotide-evoked exocytosis. *J. Cell Sci.* **115**, 3909-3922.
Tsujimoto, T., Jeromin, A., Saitoh, N., Roder, J. C. and Takahashi, T. (2002). Neuronal calcium sensor 1 and activity-dependent facilitation of P/Q-type calcium currents at presynaptic nerve terminals. *Science* **295**, 2276-2279.
Uesaka, N., Hirai, S., Maruyama, T., Ruthazer, E. S. and Yamamoto, N. (2005). Activity dependence of cortical axon branch formation: a morphological and electrophysiological study using organotypic slice cultures. *J. Neurosci.* **25**, 1-9.
Vives, E., Brodin, P. and Lebleu, B. (1997). A truncated HIV-1 Tat protein basic domain rapidly translocates through the plasma membrane and accumulates in the cell nucleus. *J. Biol. Chem.* **272**, 16010-16017.
Vocero-Akbani, A., Lissy, N. A. and Dowdy, S. F. (2000). Transduction of full-length Tat fusion proteins directly into mammalian cells: analysis of T cell receptor activation-induced cell death. *Meth. Enzymol.* **322**, 508-521.
Wang, C. Y., Yang, F., He, X., Chow, A., Du, J., Russell, J. T. and Lu, B. (2001). Ca(2+) binding protein frequenin mediates GDNF-induced potentiation of Ca(2+) channels and transmitter release. *Neuron* **32**, 99-112.
Weiss, J. L. and Burgoyne, R. D. (2001). Voltage-independent inhibition of P/Q-type Ca2+ channels in adrenal chromaffin cells via a neuronal Ca2+ sensor-1-dependent pathway involves Src family tyrosine kinase. *J. Biol. Chem.* **276**, 44804-44811.
Weiss, J. L., Archer, D. A. and Burgoyne, R. D. (2000). Neuronal Ca2+ sensor-1/frequenin functions in an autocrine pathway regulating Ca2+ channels in bovine adrenal chromaffin cells. *J. Biol. Chem.* **275**, 40082-40087.
Wood, M. R., DeBin, J., Strichartz, G. R. and Pfenninger, K. H. (1992). Plasmalemmal insertion and modification of sodium channels at the nerve growth cone. *J. Neurosci.* **12**, 2948-2959.
Zhao, X., Varnai, P., Tuymetova, G., Balla, A., Toth, Z. E., Oker-Blom, C., Roder, J., Jeromin, A. and Balla, T. (2001). Interaction of neuronal calcium sensor-1 (NCS-1) with phosphatidylinositol 4-kinase beta stimulates lipid kinase activity and affects membrane trafficking in COS-7 cells. *J. Biol. Chem.* **276**, 40183-40189.
Zheng, J. Q. (2000). Turning of nerve growth cones induced by localized increases in intracellular calcium ions. *Nature* **403**, 89-93.